frontiers | Frontiers in Materials

TYPE Original Research
PUBLISHED 14 May 2025
DOI 10.3389/fmats.2025.1550323

OPEN ACCESS

EDITED BY
Wang Zheng,
Chinese Academy of Sciences (CAS), China

REVIEWED BY
Guo Huanling,
First Affiliated Hospital of Sun Yat-Sen University, China
Dong Wang,
First Affiliated Hospital of Chongqing Medical University, China

*CORRESPONDENCE
Haiyan Yang,
629876820@qq.com
Jianzhong Zou,
zoujzh@cqmu.edu.cn

RECEIVED 23 December 2024
ACCEPTED 21 April 2025
PUBLISHED 14 May 2025

CITATION
Ou X, Tang Y, Yang H, Du Y, Zhang Z, Lin L, Wang Q and Zou J (2025) Evaluation of multimodal imaging guided multifunctional bio-targeted reactive oxygen species production synergists: a preliminary study. *Front. Mater.* 12:1550323. doi: 10.3389/fmats.2025.1550323

Evaluation of multimodal imaging guided multifunctional bio-targeted reactive oxygen species production synergists: a preliminary study

Xia Ou[1,2], Yu Tang[2], Haiyan Yang[1,2]*, Yan Du[2], Zhong Zhang[2], Li Lin[2], Qi Wang[2] and Jianzhong Zou[2]*

[1]Chongqing General Hospital, Chongqing University, Chongqing, China, [2]State Key Laboratory of Ultrasound in Medicine and Engineering, Chongqing Medical University, Chongqing, China

Objective: Pulse focused ultrasound (PFUS) is facing the big challenge of rapid attenuation of ultrasonic energy. Although synergists existed are helpful, they have limitations such as poor targeting, incomplete imaging during therapy, and tumor residue after therapy. This study aims to construct bio-targeted reactive oxygen species (ROS)- producing synergists (abbreviated as B.*bifidum*@PC-CLs) consisting of Bifidobacterium bifidum (B. *bifidum*) and multifunctional ROS producing nanoparticles (abbreviated as PC-CLs) loaded with chlorin e6 (Ce6) a multifunctional nd perfuorohexane (PFH), which is expected to make up for the shortcomings of existing PFUS collaborative therapy, and provide an idea for tumor diagnosis and treatment.

Methods: The PC-CLs were prepared for testing the capability of multimodal imaging, ROS production and SDT intracellular, and synergistic effect *in vitro*. The tumor-targeted ability of B.*bifidum*@PC-CLs was detected through electrostatic adsorption. The synergistic therapy and antitumor therapy of B.*bifidum*@PC-CLs with PFUS were analyzed *in vivo*.

Methods: Studies validated that PC-CLs have excellent abilities of multimodal imaging, ROS-producing and SDT-enhancing. Moreover, B.*bifidum* could not only actively target 4T1 tumor and prolify itself, but also facilitate the delivery and retain of PC-CLs in tumor during electrostatic adsorption. Importantly, B.*bifidum*@PC-CLs amplified cavitation effect and PFUS-SDT combined antitumor effect.

Conclusion: A multifunctional bio-targeted B.*bifidum*@PC-CLs was constructed successful, which may provide an unique nanoparticle platform to guide PFUS for efficient and safety tumor treatment.

KEYWORDS

PFUS, bio-targeted, ROS, SDT, multimodal imaging

Introduction

The precise and safe tumor therapy is currently a hot topic (Li et al., 2022a; Mai et al., 2021). Pulse focused ultrasound (PFUS) has shown great potential in clinical

treatment of solid tumors (Ou et al., 2023). PFUS can disintegrate and homogenize tumor tissue precisely and achieve therapeutic effect through various biological effects, mainly mechanical effect and cavitation effect, which do not cause worrying thermal completions, such as skin burn (Wang et al., 2020a; Li et al., 2023; Ruger et al., 2023). However, the efficiency of PFUS in large and deep tumor tissues will be affected because of the attenuation characteristic of ultrasound (Jiang et al., 2022). Kinds of synergistic agents were used to increase the efficiency of PFUS therapy and minimize treatment times. The most widely used substances are phase-transitional lipid nanoparticles (NPs) consisting of quid fluorocarbon perfluorohexane (PFH) with reliable biosafety and stable liquid-gas phase transition, which was applied for focused ultrasound to increase cavitation effect to destroy tumor cells and tissues (Zeng et al., 2022; Khella et al., 2022; Yang et al., 2020). Besides, PFH can be stimulated by ultrasound (US) and transform into a large of microbubbles, acting as cavitation nucleus to enhance the US imaging (Qiu et al., 2023; Li et al., 2014).

Although the use of phase-transitional lipid NPs improves the curative effects of PFUS, the targeting of PFH lipid NPs present a magnitude challenge at present. Poor targeting NPs will spread with bloodstream throughout the body, leading to low synergism and organism damage (Zhao et al., 2022). Researchers believed that NPs targeting can be improved by specific chemical modification. However, the poor stability and availability of modification in the bloodstream, and the diversity of tumors both increase the off-target probability of NPs (Mcgranahan and Swanton, 2017; Martino et al., 2023). Therefore, a highly efficient tumor targeted delivery plays an important role to assist PFUS in achieving precision therapy of solid tumors. Given the hypoxic microenvironment of solid tumors and the growth characteristics of anaerobic bacteria, biological carriers provide a new strategy for targeted treatment. Bifidobacterium, a probiotic, maybe a better choice among them due to its unique properties, which not only can be used as carriers for targeted treatment without altering its own characteristics, but also have anti-tumor effects (Wang et al., 2020b; Kikuchi et al., 2017; Kim et al., 2022; Benito et al., 2021). Specifically, Bifidobacterium is a kind of human probiotic that will not lead to immunological or pathogenic risk (Fukiya et al., 2012). Secondly, the anaerobic and acidophilic properties of Bifidobacterium make it easy to accumulate and proliferate into tumor microenvironment which exactly meet its metabolic needs (Shi et al., 2023; Ippolito et al., 2019). Third, Bifidobacterium can disrupt tumor cells and inhibit its growth (Jiang et al., 2022; Li et al., 2022b). In fact, there are many species of Bifidobacterium. Compared to other strains, Bifidobacterium bifidum (B.*bifidum*) has several advantages, such as more safety on the host, easy to obtain and so on (Kim et al., 2021).

Another key problem is the real-time visualization of NPs distribution in tumor, otherwise it is difficult to evaluate the PFUS therapeutic effect properly. Compare to a single imaging, multi-mode can offer much more rich information and be of significant value to provide dynamics of tumor progression for the accurate location of therapeutic focusing spot in targeted tissue, showing great potential in clinical therapy (Luo et al., 2022; Cheng et al., 2023; Ran et al., 2023). Especially photoacoustic (PA) imaging and fluorescence (FL) imaging, they have distinctive advantages in terms of sensitivity and penetration depth compared to commonly US imaging, giving it a critical complementarity for PFUS imaging monitoring (He et al., 2021). With the increase of combination therapy, NPs is becoming increasingly multifunctional to meet clinical demand so as to reduce the tumor recurrence. Chlorin e6 (Ce6), a derivative of natural chlorophyll, not only has excellent PA and FL imaging ability because of its absorbance peak at 680 nm and auto-fluorescence property (Zhang et al., 2022), but also serves as a sonosensitizer for sonodynamic therapy (SDT) due to its reactive oxygen species (ROS) generation effect (Shan et al., 2024). SDT is a promising therapeutic method for tumor, which involves sonosensitizers triggered by US and has many advantages including high penetration, high precision, and bare side effect (Huang et al., 2024; Dong et al., 2023). The production of a large amount of ROS during SDT may reduce proliferative activity of tumor cells and prompt their apoptosis (Tian et al., 2024). Therefore, choosing NPs containing Ce6 as imaging agents and sonosensitizers will kill two birds with one stone, realizing multimodal imaging and complementary therapy.

To sum up, our study designed and synthesized bio-targeted synergists to solve the above problems. As shown in Scheme 1, the synergist consisted of bio-targeted carriers B. *bifidum* and multifunctional ROS-producing NPs loaded with PFH and Ce6 (CL-PFH-Ce6-NPs, herein after referred to as PC-CLs). In order to minimize the impact of modification on B. *bifidum* and to maximize the delivery efficiency on lipid NPs, we chose electrostatic adsorption mode to couple with B. *bifidum* and NPs, and a two-step delivery method *in vivo* was used (Kikuchi et al., 2017; Wang et al., 2023). It is hypothesized that with the guidance of electrostatic adsorption, the bio-targeted ROS production synergists will achieve self-assembly in the tumor and enhance the effect of PFUS treatment, thereby provide a potential application opportunity. The bio-targeted synergists showed distinctive features beneficial for tumor therapy: (i) it not only had good biocompatibility, but also could actively target most types of solid tumors and inhibit tumor growth; (ii) enhanced accumulation and prolonged circulation itself through continuous electrostatic adsorption guidance; (iii) real-time monitoring during multimodality imaging; (iv) a PFUS-responsive strategy for stimulating NPs loaded with PFH and Ce6 in tumor site, on the one hand, which realized a cascade amplification cavitation effect due to more and rapid cavitation nucleus generation, on the other hand, ROS produced by Ce6 leaded to SDT and destroyed residual tumors and enhanced antitumor therapy.

Experiment

Materials

1,2-dipalmitoyl-sn-glycero-3-phosphocholine (DPPC), DC-cholesterol hydrochloride (DC-CHOL), and 1,2-distearoyl-sn-glycero-3-phosphoethanola mine-N-[amino (polyethyleneglycol)-2000] (DSPE-PEG 2000-Amine) were all obtained from Avanti Polar Lipids (United States). Chloroform ($CHCl_3$) was purchased from Chuandong Chemical Group (China). Chlorin e6(Ce6) and 2′,7′-dichlorodihydrofluorescein diacetate (H2DCFDA) were obtained from Beyotime (Shanghai). Fluorescein isothiocyanate

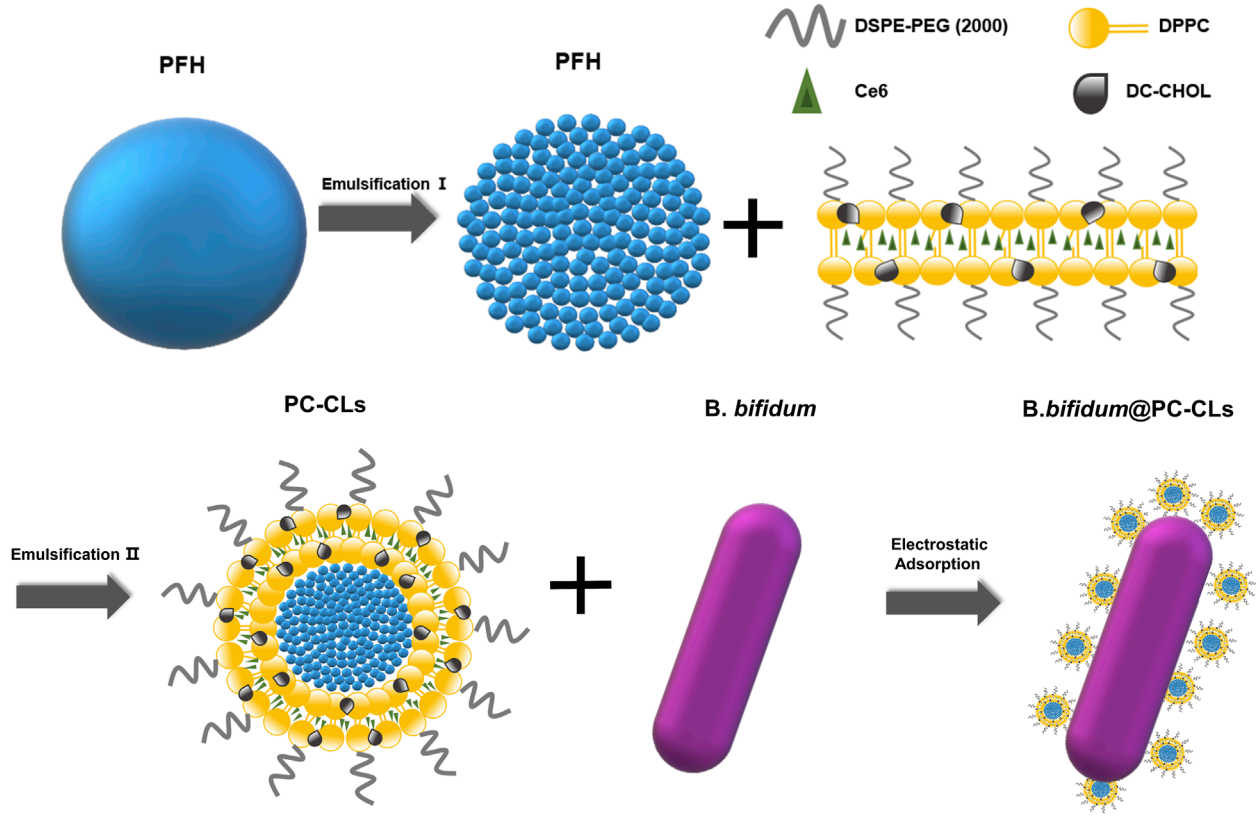

SCHEME 1
Diagram of the synthesis procedure of B. *bifidum*@PC-CLs.

(FITC), 1.1′dioctadecy3,3,3′-tetramethylindocarbocyaninepercholrate (Dil), Cell counting kit-8 (CCK-8) and 4,6-Diamidino-2-phenylindole (DAPI) were purchased from BioFrox (Germany). Perfluorohexane (PFH) was purchased from Aladdin (China). Aalcein-AM/propidium iodide (Aalcein-AM/PI) was obtained from Dojindo (Japen).B.*bifidum* (ATCC29521) was obtained from Type Culture Collection (United States)and 4T1 breast tumor cells was purchased from Cell Bank of Chinese Academy of Sciences.

Synthesis of multi-functional ROS producing nanoparticles

A two-step emulsion method was taken for more uniform NPs (Jian et al., 2014). DPPC, DC-CHOL, DSPE-PEG (2000)-amine and Ce6 were dissolved in $CHCl_3$ at the weight ratio of 6:2:2:3, and then rotated and evaporated under reduced pressure at 40°C to form thin film of lipid layer. Fifty minutes later, 2 mL of deionized water was added to hydrate the film.0.2 mL of PFH was added into 1 mL deionized water and sonicated at 100 w under ice bath condition for the first homogeneous emulsification. Then, the PFH emulsion was added into lipid layer and emulsified for the second time at 120 w under the same conditions. Next, the suspension was filtered through a microporous membrane to obtain the PC-CLs loaded with PFH and Ce6. The P-CLs only equipped with PFH were obtained by not adding Ce6 during the preparation process. DC-CHOL was replaced with cholesterol to synthesize PC-Ls equipped with PFH and Ce6. The fluorescent NPs were obtained by adding Dil to $CHCl_3$.

Culture of B. *bifidum*

The B. *bifidum* strain was cultured at 37°C in Man-Rogosa-Sharpe (MRS) broth for 24 h and purified by low temperature centrifugation (4°C, 4,000 rpm, 10 min). After that, the concentration of B. *bifidum* was adjusted to 10^6 CFU/mL with phosphate-buffered saline (PBS, pH 7.4) for further use.

Characterization of multi-functional ROS producing nanoparticles and B. *bifidum*

Transmission electron microscopy (TEM) (Hitachi 7500) was used to observe the internal structure of PC-CLs. The morphology of B. *bifidum* was observed by optical microscope (OM) (Olympus CX22) after gram staining. The mean particle sizes of PC-CLs and B. *bifidum* were measured with DLS Nanometer (NanoDLS NY). With the UV spectrophotometer (Varioskan LUX), the absorbance of PC-CLs, Ce6 were detected, and standard curves was obtained at 404 nm absorption wavelength for Ce6.

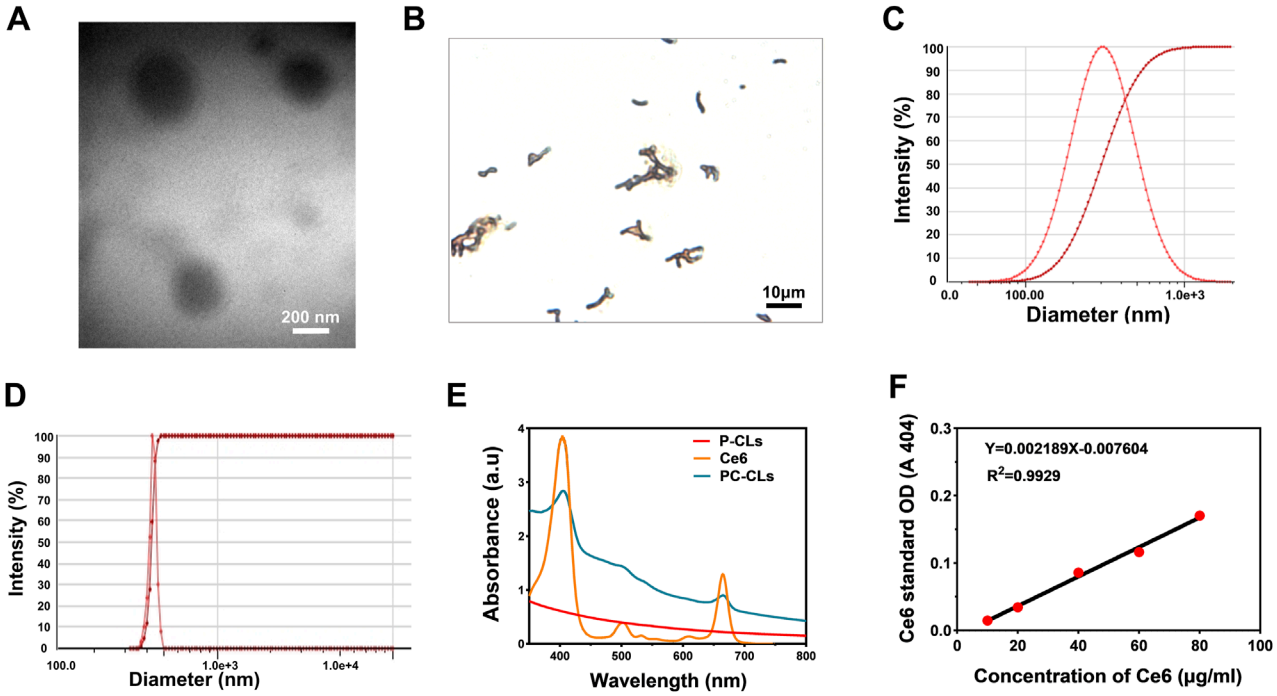

FIGURE 1
Characterization of PC-CLs and B. *bifidum*. **(A)** TEM image of PC-CLs. **(B)** Gram staining of B. *bifidum*. **(C)** One of the size distribution of PC-CLs (n = 3). **(D)** One of the size distribution of B. *bifidum* (n = 3). **(E)** UV spectra of free Ce6, P-CLs and PC-CLs and **(F)** The calibration curve of Ce6 with different concentration.

Construction of the bio-targeted ROS producing synergists

In order to construct the bio-targeted ROS producing synergists, PC-CLs (l mg/mL) were mixed with B. *bifidum* (10^6 CFU/mL) at a ratio of 2:1 v:v, and the solution reacted for 5 min. The zeta potential and particle size of bio-targeted ROS producing synergists were measured.

To observe the absorption between PC-CLs and B. *bifidum*, PC-CLs and PC-Ls (both l mg/mL) were labeled with Dil, and B. *bifidum* (10^6 CFU/mL) were labeled with FITC. Bio-targeted group (B.*bifidum* + PC-CLs) and non-targeted group (B.*bifidum* + PC-Ls) were observed via confocal laser scanning microscopy (CLSM) (Nikon Microsystems), judging the coupling effect between B. *bifidum* and NPs. The flow cytometry (FCM) (FACSVantage SE) was used to confirm the coupling efficiency of the two groups.

Multimodal imaging of PC-CLs *in vitro*

To evaluate the US imaging capability of multifunctional ROS producing nanoparticles, 0.2 mL of PBS and PC-CLs solution (l mg/mL) were added to an agar gel phantom. The Model-JC200 focused ultrasound tumor therapeutic system (Chongqing Haifu Medical Technology Co., Ltd.) was used for PFUS with the following parameters: frequency 1.0 MHz; power 4 w; irradiation time 30 s; duty cycle 10%. US imaging before and after PFUS were detected in B mode and Contrast mode, and the echo intensity (EI) was analyzed.

Similarly, 0.2 mL of PBS and different concentrations of PC-CLs were tested for PA imaging, the change of PA signal in different solution was observed using Vevo LASER PA imaging system (Visual Sonic) at a frequency of 21 MHz and wavelength of 795 nm.

FL imaging was conducted on spectrum imaging system (Berthold LB983) using an excitation wavelength of 660 nm and a filter of 800 nm. PC-CLs solution with different concentrations was placed into 96- well plates sequentially. The FL average values were taken via the built-in software of spectrum imaging system.

4T1 cell culture and tumor-bearing mouse models

The cells were cultured at 37°C with 5% CO_2 in RPMI-1640 medium supplemented with 10% fetal bovine serum (FBS) and 1% streptomycin/penicillin.

Each animal procedure was carried out with the Guidelines for Care and Use of Laboratory Animals of Chongqing Medical University. To establish the tumor model, 0.1 mL 4T1 tumor cells (about 1×10^6) suspension was subcutaneously injected into the buttocks of BALB/C mouse (female, 20–23 g) as previously described (Luo et al., 2019). When the tumor diameter reached about 8 mm, *in vivo* experiments were performed.

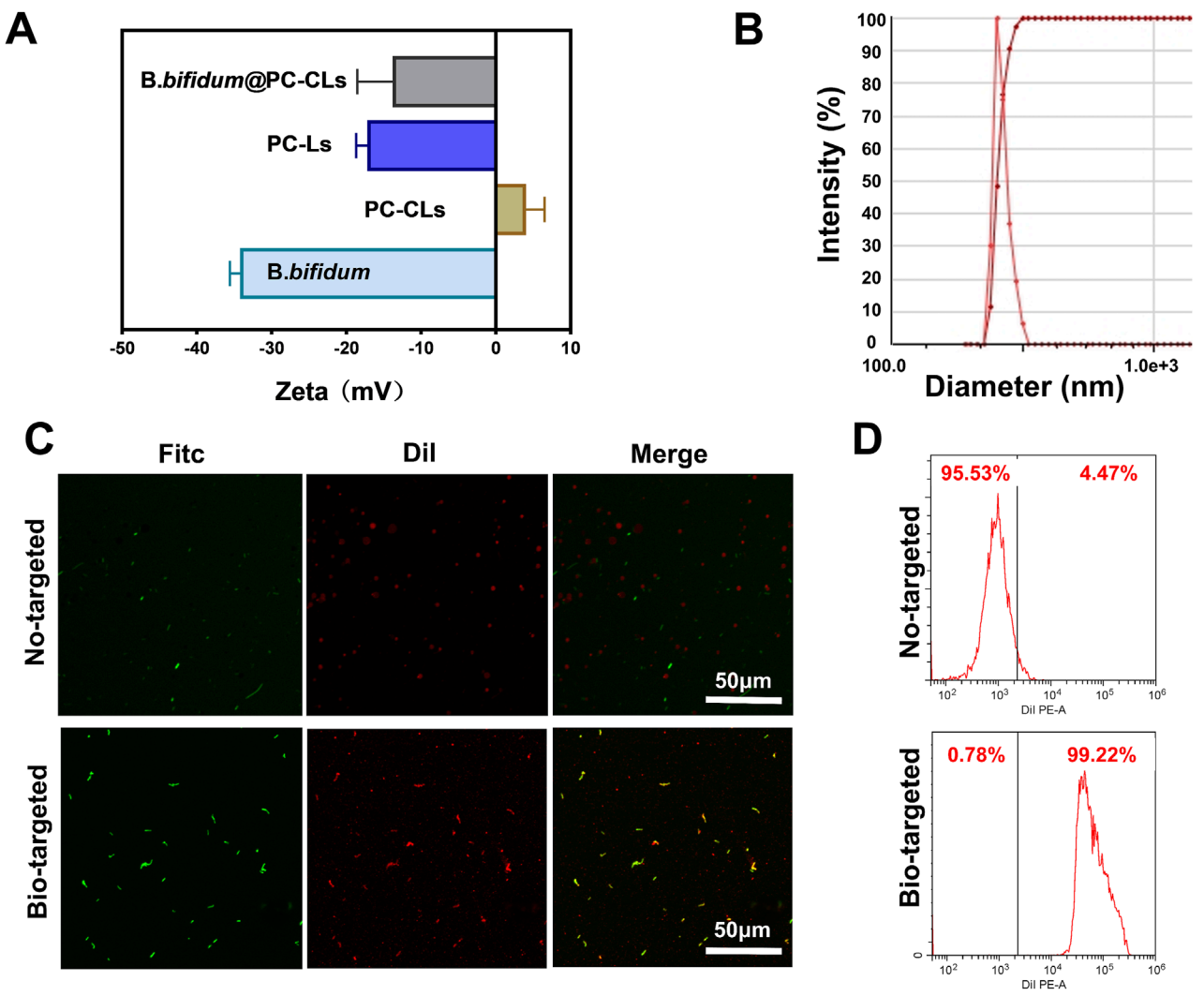

FIGURE 2
Construction of the Bio-targeted ROS producing synergists. **(A)** Surface zeta potential of PC-Ls, PC-CLs, B. *bifidum* and Bio-targeted ROS producing synergists (B. *bifidum*@PC-CLs). **(B)** One of the size distribution of B. *bifidum*@PC-CLs (n = 3). **(C)** CLSM images and **(D)** FCM results of B. *bifidum* mixing with PC-CLs and with PC-Ls, respectively.

TABLE 1 Zeta Potential (Mean ± SD, n = 3).

Substance	Value (mV)
B. *bifidum*	−34.2 ± 1.2
PC-Ls	−17.2 ± 1.5
PC-CLs	4.0 ± 2.4
B.*bifidum*@ PC-CLs	−13.8 ± 4.7

The ability to produce ROS intracellular of PC-CLs

H2DCFDA (a fluorescent probe used for detecting the generation of ROS) was used to assess the ROS production intracellular in P-CLs group and PC-CLs group.

4T1 breast tumor cells in logarithmic growth phase were inoculated into confocal dishes for 24 h and divided into four duty cycles:2%,5%,10% and 20%, and followed by co-incubation with 0.2 mL of P-CLs solution or PC-CLs solution (both l mg/mL) for 1 h. Then, each dish was subjected to PFUS at a power of 4 w for 30 s with corresponding duty cycle. Next, 0.1 mL of H2DCFDA was added into dishes and incubated in dark for 15 min, then observed via CLSM.

SDT of PC-CLs *in vitro*

To further assess the ability of PC-CLs for SDT, 4T1 tumor cells in logarithmic growth phase inoculated into confocal dishes (approximately 1×10^3 cells per dish) were randomly allocated to six group: (1) PBS; (2) Ce6; (3) PC-CLs; (4) PBS + PFUS; (5) Ce6 + PFUS; (6) PC-CLs + PFUS. Each dish of every group was added

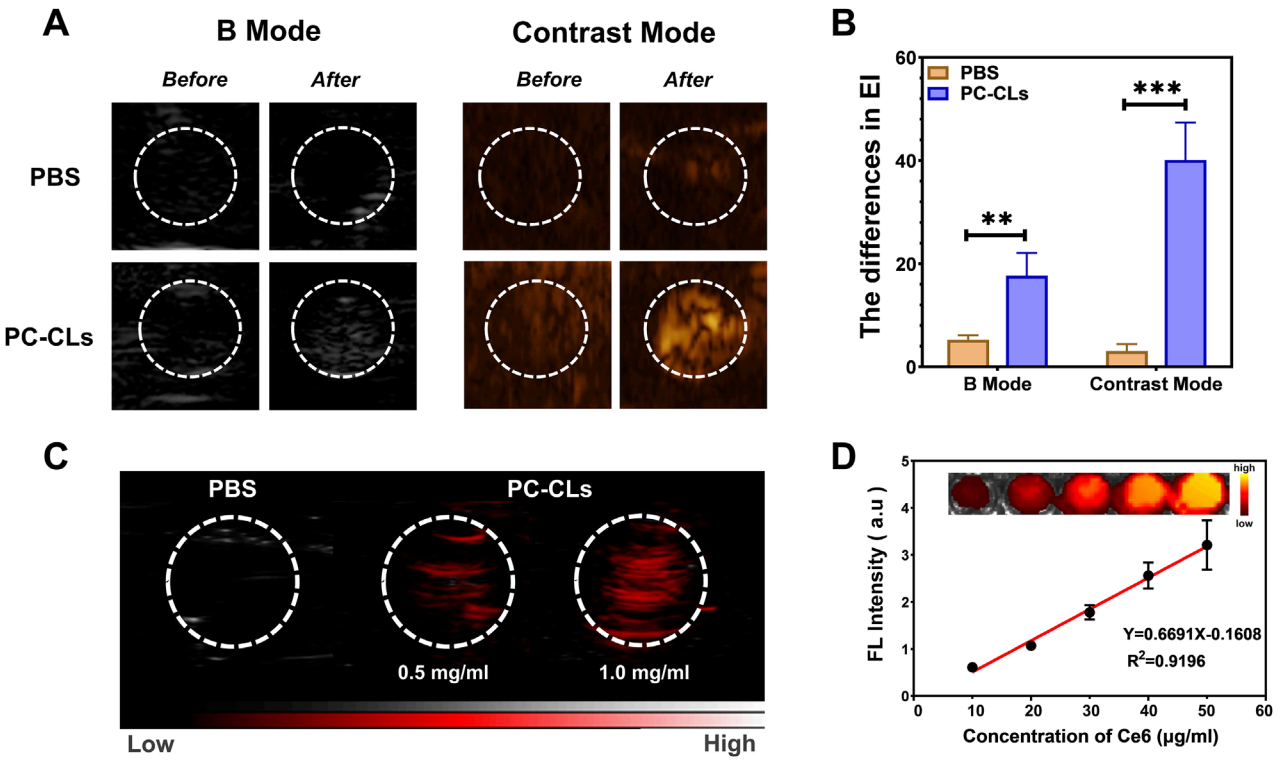

FIGURE 3
Multi-modal imaging of multi-functional ROS producing NPs (PC-CLs) *in vitro*. **(A)** Ultrasound images and **(B)** Quantitative analysis of EI in B mode and Contrast mode before and after PFUS of PBS group and PC-CLs group (n = 3). There was a significant increase in both modes in PC-CLs compared with PBS (***P* < 0.01,****P* < 0.001). **(C)** PA images of PBS and PC-CLs. **(D)** FL image of different Ce6 concentrations, and the linear relationship between the FL signal value with the concentration.

into 0.1 mL of responding solution (1 mg/mL). Next, the last three groups were irradiated with PFUS (1.0 MHz, 4 w, 30 s, 10%). The cells of every group were incubated with 0.1 mL of prepared calcein-AM/P solution for 20 min at 37°C. The viable and dead cells were distinguished based on their fluorescent staining patterns, which could be visually observed and counted via CLSM. The dead cells were further accounted.

Synergistic effect of PC-CLs with PFUS

To test the synergistic efficacy of multi-functional ROS producing nanoparticles *ex vivo*, 0.2 mL of PBS, B. *bifidum* (10^6 CFU/mL) solution and PC-CLs (l mg/mL) solution were injected into degassed bovine liver tissue separately under US monitor instrument. The grayscale value change of liver tissue before and after PFUS (Model-JC200 Focused Ultrasound Tumor Therapeutic System, 1.0 MHz, 120 w, 30 s, 10%) and the necrotic morphology were both recorded. The ablation volumes were calculated using the HifuJupiter F software and according to the following formulas:

$$V\left(mm^3\right) = (\pi/6) \times length \times width \times depth.$$

Targeted detection of bio-targeted ROS producing synergists

Nine 4T1 breast tumor-bearing mice were randomly divided into the Control group, 3 days group and 7 days group. The mice in the last two groups were tail vein injected with 0.2 mL B. *bifidum* suspension (10^6/mL) for three consecutive days. While mice in Control group were injected with 0.2 mL PBS. At post-3 and post-7 days after injection, the mice in the corresponding group were sacrificed, and the tumor and major organs were extracted and fixed in paraformaldehyde. The tissues subjected to section and gram staining, the distribution of B. *bifidum in vivo* tissues was observed by a OM (Olympus CX22).

Tumor-bearing mice were randomly allocated to bio-targeted group and non-targeted group (twelve mice/group). The mice in the bio-targeted group were injected with 0.2 mL of B. *bifidum* for three consecutive days. Similarly, the mice in the non-targeted group were treated with 0.2 mL PBS. On day 7 after injection, mice in both groups were injected with 0.2 mL PC-CLs (1 mg/mL) intravenously. Mice of the two groups were sacrificed at 6 h, 12 h, 24 h and 48 h after PC-CLs injection. Tumors were harvested to make ultra-thin sections and labeled with DAPI, observing via CLSM to assess the targeting ability of bio-targeted ROS producing synergists.

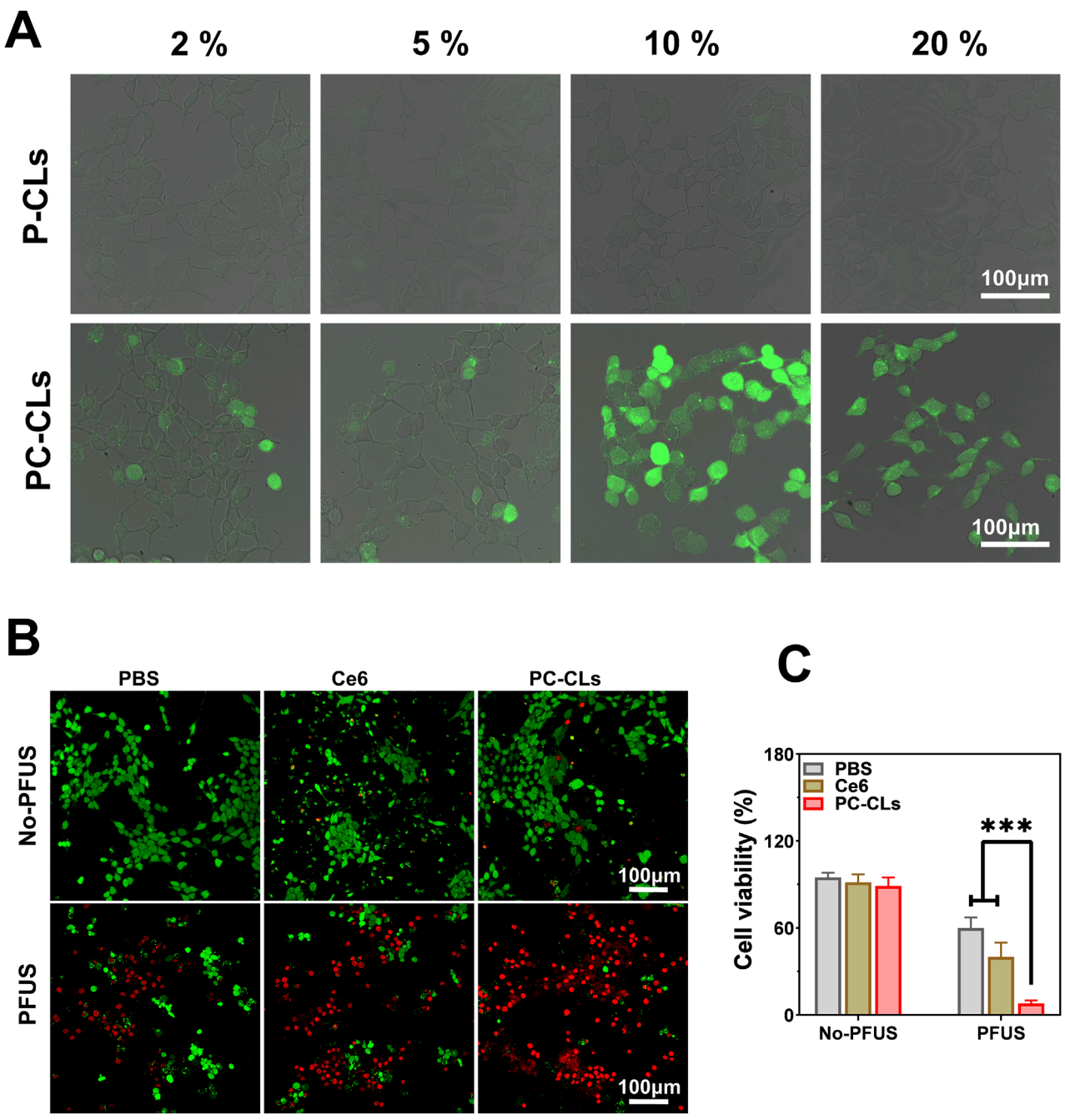

FIGURE 4
The ROS producing and SDT capability of PC-CLs intracellular. **(A)** CLSM images of PC-CLs group and P-CLs group after PFUS with different duty cycles. **(B)** CLSM images of PBS group, Ce6 group and PC-CLs group with or without PFUS. **(C)** Analysis of cells viability rates of different groups (n = 3). Compared with other two groups, cells viability rates of PC-CLs group with PFUS was significant low (***$P < 0.001$).

Synergistic therapy of B. *bifidum*@PC-CLs with PFUS

PBS group, B. *bifidum* group, PC-CLs group, and B. *bifidum*@PC-CLs group with five mice each to evaluate synergistic capability of the bio-targeted ROS producing synergists *in vivo*. At first, the mice in B. *bifidum* and B. *bifidum*@PC-CLs group were injected with 0.2 mL of B. *bifidum* (10^6/mL) suspension intravenously for three consecutive days. Mice in other two groups were injected with the same volume PBS. On day 7 after injection, 0.2 mL PBS was injected into the mice of PBS group and B. *bifidum* group, while 0.2 mL of PC-CLs (1 mg/mL) were injected into the mice of PC-CLs group and B. *bifidum*@PC-CLs group respectively. PFUS was performed under US guidance. The ultrasonic images of the tumor target area were recorded, and the gray change values before and after therapy were calculated. All mice were sacrificed,

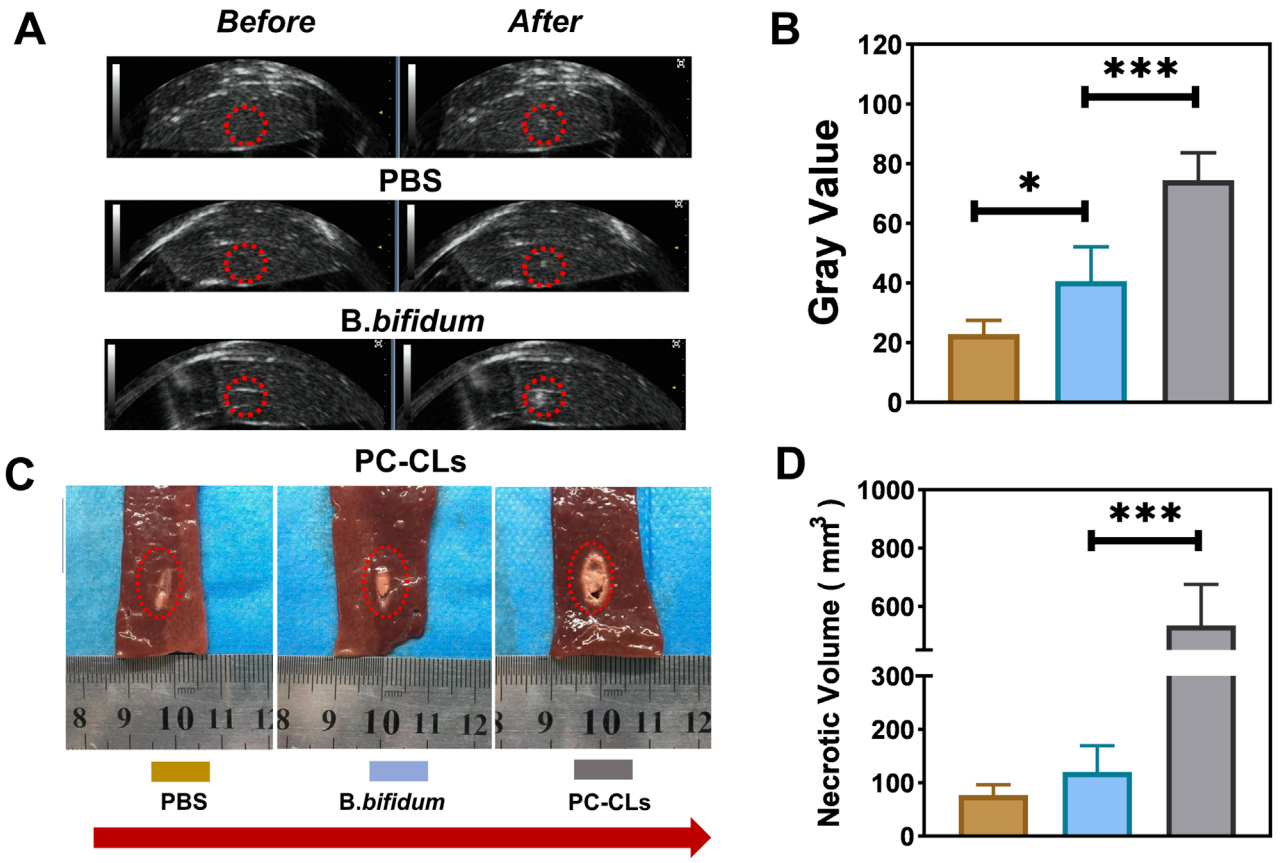

FIGURE 5
Synergistic effect of PC-CLs with PFUS. **(A)** US image of liver tissue before and after PFUS and **(B)** Quantitative analysis of grayscale value change of liver tissue in PBS group, B. *bifidum* group and PC-CLs group (n = 5). **(C)** Necrotic morphology and **(D)** Necrosis volume (n = 5). Compared with other two groups, gray value and necrosis volume of liver tissue in PC-CLs group were both evident large (***$P < 0.001$).

the tumors were harvested to evaluate the necrosis degree of the tumor with TTC staining (37°C, 30 min), and the necrosis volume and energy efficiency factor (EEF) were calculated with the following formula.

$$V\left(mm^3\right) = (\pi/6) \times length \times width \times depth.$$

$$EEF\left(J/mm^3\right) = \eta Pt/V\left(\eta = 0.7, P = 120\,w, t = 30\,s\right)$$

Antitumor therapy of B. *bifidum*@PC-CLs with PFUS

To verify PFUS-SDT combined antitumor effect *in vivo*, the mice were allocated and treated the same as synergistic therapy experience *in vivo*. Tumor volume was measured every 4 days from the day of therapy. The relative tumor volume (RTV) was normalized, the initial tumor volume before therapy was used as standardized, RTV was therapy one/initial one. On day 17 after therapy, mice were sacrificed, and tumors were harvested and measured before staining with hematoxylin-eosin (HE), nuclear proliferation-associated antigen (Ki-67) and terminal deoxynucleotide transferase-mediated end-incision labeling (TUNEL).

Biosafety assessment

As a test of biocompatibility for PC-CLs, hemolysis was detected. Blood samples were tested to assay the biosafety of bio-targeted ROS producing synergists *in vivo* within a 14 days-term, including complete blood count and markers of liver and kidney function. The major organs of the mice injected with the bio-targeted ROS-producing synergists above and of mice untreated were stained with HE to determine the safety for tissue.

Statistical analysis

GraphPad Prism version 8.0 was used for all the statistical analyses. Continuous data were expressed as mean ± standard deviation (SD). The *t*-test and one-way analysis of variance were applied for analyzing data. $P < 0.05$ was set as statistical significance.

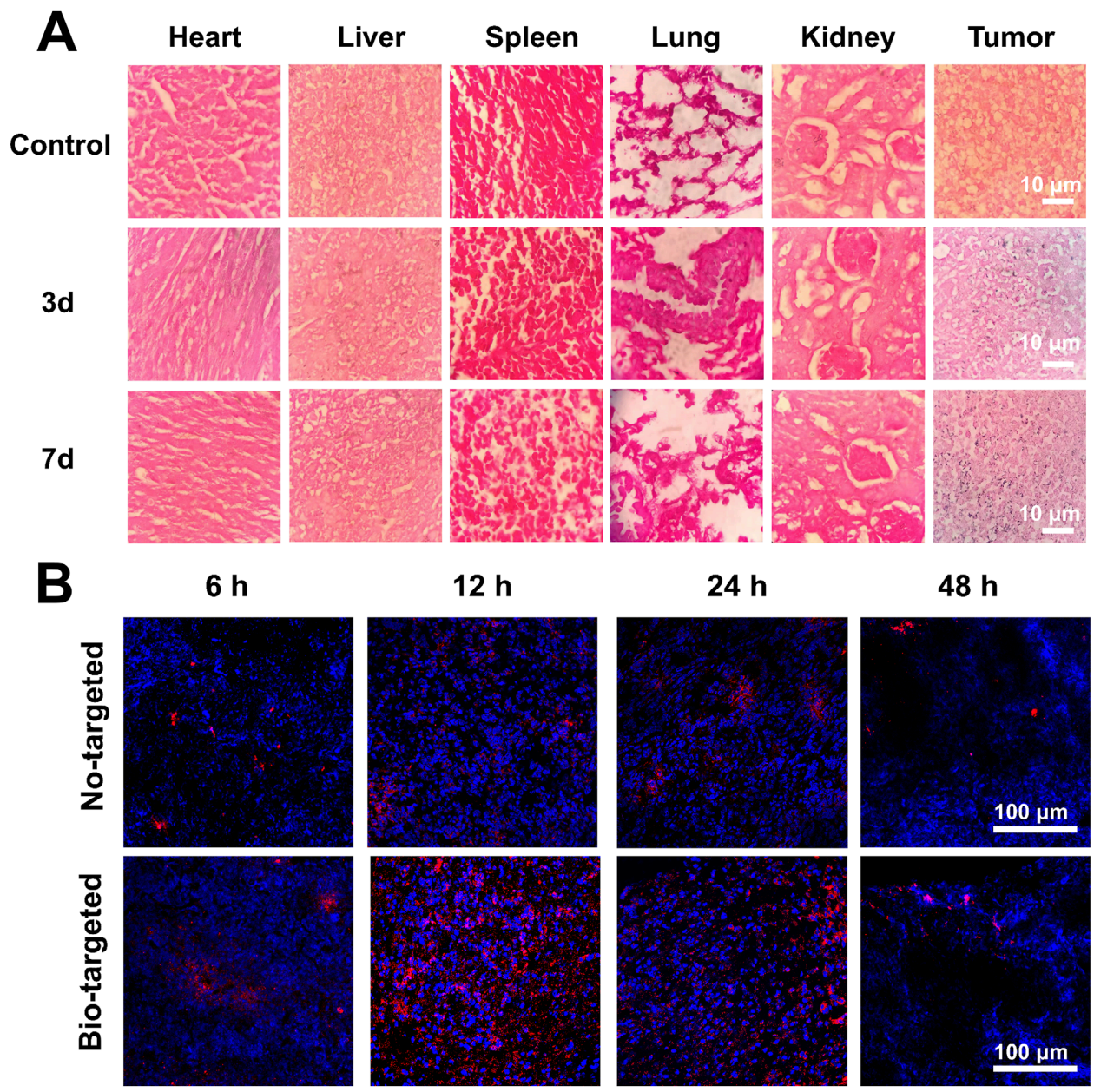

FIGURE 6
Targeted detection of bio-targeted ROS producing synergists. **(A)** The colonization of B. *bifidum* in various tissues after gram staining **(B)** CLSM images of ultra-thin section of tumor tissues at 6 h, 12 h, 24 h and 48 h after injection of PC-CLs or B. *bifidum*@PC-CLs (Bio-targeted ROS producing synergists).

Results

Morphological and basic characteristic

PC-CLs encapsulated with hydrophobicity Ce6 in the membrane layer and inert PFH as the core of the NPs (Scheme 1). The TEM images of PC-CLs displayed spherical shape with fine dispersity as shown in Figure 1A, and the lipid film including DPPC, DC-CHOL and DSPE-PEG (2000) was uniform. B. *bifidum* presented as short rods in the field of OM (Figure 1B). The mean diameter of PC-CLs and B. *bifidum* was 292.7 ± 12.2 nm (Figure 1C) and 1,374.0 ± 1,394.3 nm (Figure 1D)respectively. The UV absorption spectra indicated that Ce6 has been successfully encapsulated in the PC-CLs (Figure 1E), and according to the Ce6 standard curve (Figure 1F), the encapsulation efficiency of Ce6 in PC-CLs was 65.04%.

Evaluation the construction of the bio-targeted ROS producing synergists

As shown in Figure 2A; Table 1, the surface potentials of B. *bifidum* and PC-Ls were negatively charged, and PC-CLs had

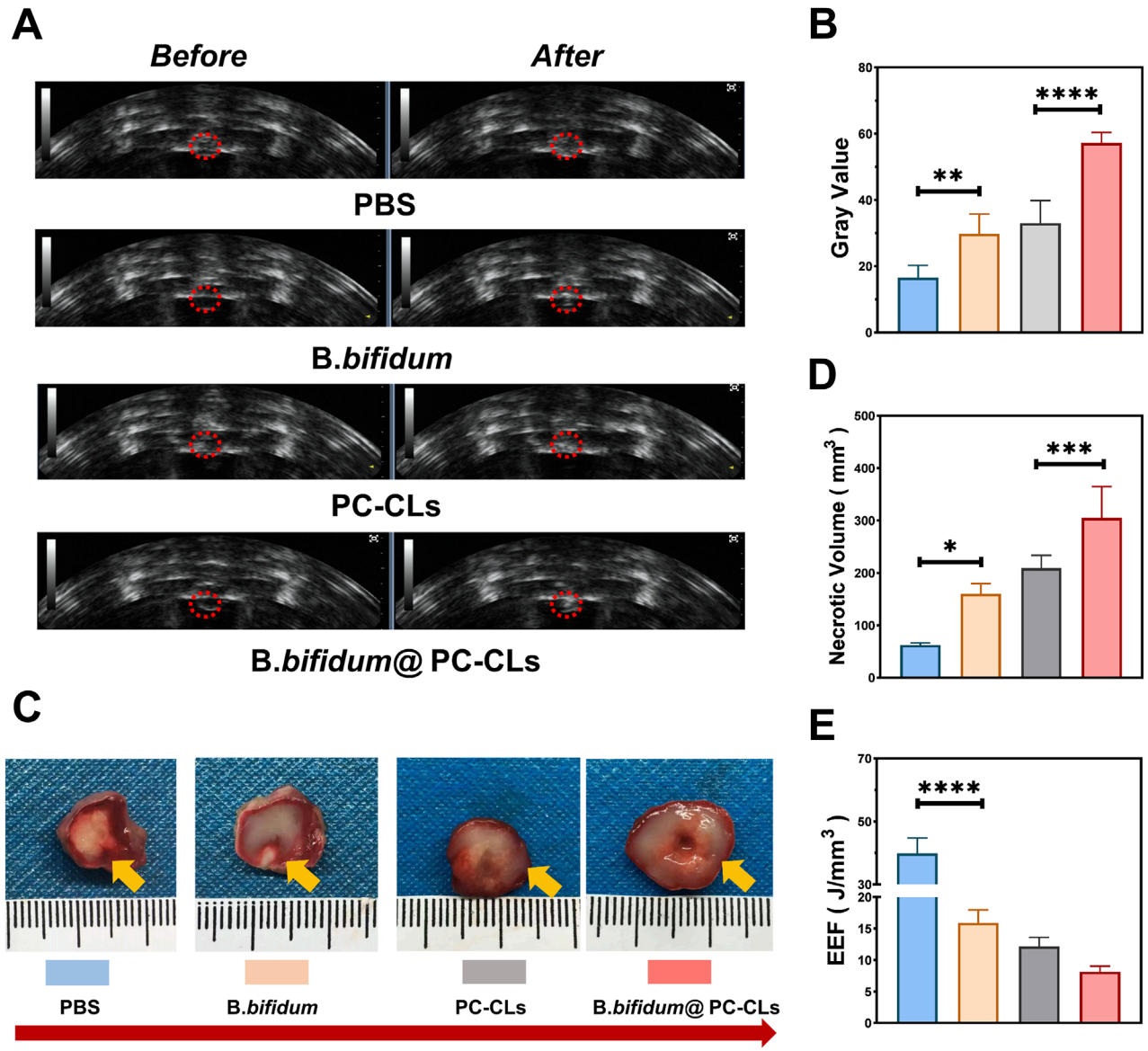

FIGURE 7
Synergistic therapy of B. *bifidum*@PC-CLs with PFUS. **(A)** US image before and after PFUS and Quantitative analysis of **(B)** grayscale change, **(D)** necrosis volume and **(E)** EEF at the targeted area in tumor. **(C)** Tumor necrotic morphology revealed by TTC staining following PFUS. Compared with other three groups, gray value and necrosis volume of tumors in B. *bifidum*@PC-CLs group were significant large (***$P < 0.001$, ****$P < 0.0001$),while EEF in B. *bifidum*@PC-CLs group was obvious small (****$P < 0.0001$).

positive potential. The potentials of B. *bifidum* and PC-CLs were opposite, which have the possibility for electrostatic adsorption. The bio-targeted ROS producing synergist was an B. *bifidum* and PC-CLs mixture with an zeta potential of −13.8 ± 4.7 mV (Table 1) and particle size of 2,174.3 ± 162.3 nm (Figure 2B).

In order to detect whether B. *bifidum* and PC-CLs are successfully coupling through electrostatic adsorption, Dil-labeled red fluorescence NPs and FITC-labeled green fluorescence B. *bifidum* were observed via CLSM (Figure 2C) intuitively. There was a large more red fluorescence on the surface of B. *bifidum* in Bio-targeted group compared with the No-targeted group, which demonstrated that the bio-targeted ROS producing synergist was successfully built through electrostatic adsorption. FCM (Figure 2D) quantified that the coupling rate of Bio-targeted group was 99.22%, while the No-targeted group was only 4.47%. It is an appropriate way that retains original character maximum by modifying the potential of NPs, which lay a foundation for subsequent internal treatment.

Multimodal imaging of PC-CLs *in vitro*

As shown in Figures 3A,B, compared with PBS group, there was a dramatic change in PC-CLs group with B mode and Contrast mode after PFUS, and the differences in EI were also statistically significant. Figure 3C depicted that PC-CLs an

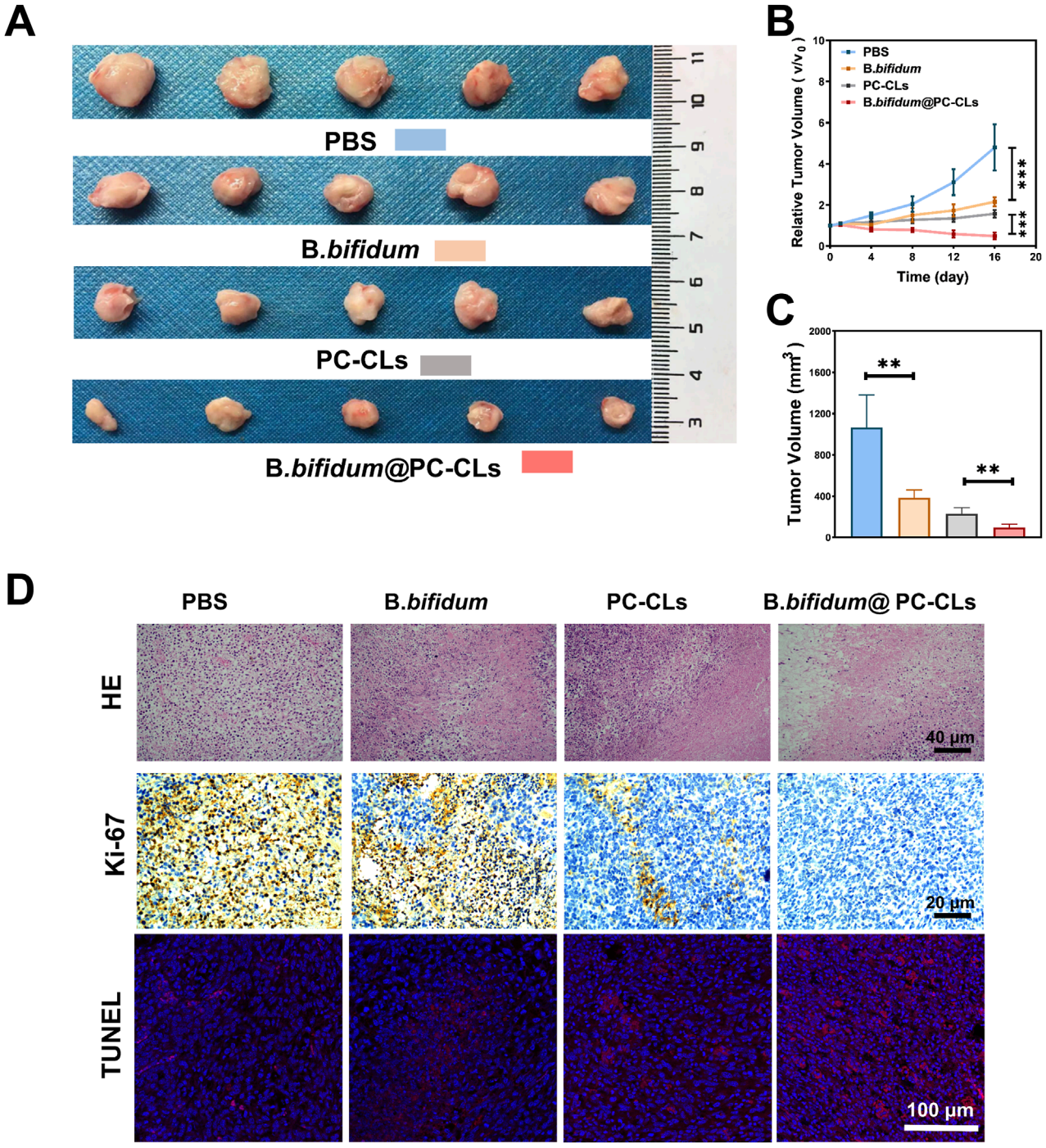

FIGURE 8
Antitumor effect of B. *bifidum*@PC-CLs with PFUS. **(A)** Tumor photos of different groups (PBS, B. *bifidum*, PC-CLs, B. *bifidum*@PC-CLs) on day 17. **(B)** Analysis of relative tumor volume and **(C)** Tumor volume on day 17 with different groups. Compared with other three groups, results of the above two indicators of B. *bifidum*@PC-CLs group were significant small (**$P < 0.01$, ***$P < 0.001$). **(D)** HE staining, Ki67 and TUNEL images of targeted area in tumor after therapy.

outstanding PA contrast agent, and the fluorescence intensity is related to concentration. Ce6 had strong absorption in the NIR region, it was clear that the FL signal generated by PC-CLs was linearly enhanced with Ce6 concentration, showing its excellent FL imaging capability because of Ce6 (Figure 3D).

The ROS producing and SDT capability of PC-CLs intracellular

H2DCFDA can rapidly convert ROS into 2′,7′-dichlorofluorescein (DCF) labeled with green fluorescent, which can be observed

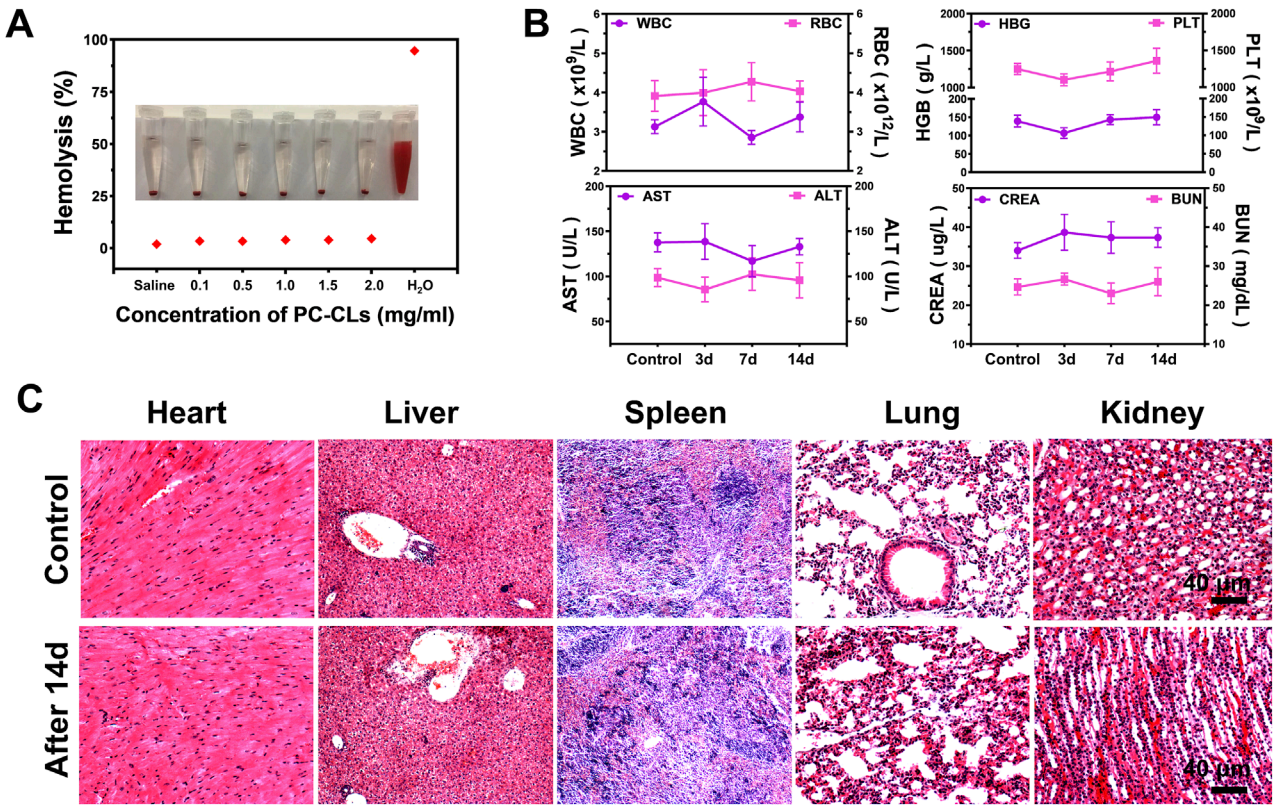

FIGURE 9
Biosafety assessment. **(A)** Hemolysis test of PC-CLs *in vitro*. **(B)** Blood routine and blood biochemical indexes at different time points after Bio-targeted ROS production synergists (B. *bifidum*@PC-CLs) injections. **(C)** HE staining images of major organs from healthy mice and mice treatment with Bio-targeted ROS production synergists after 14 days.

via CLSM. As shown in Figure 4A, green fluorescence could be seen in all images of the PC-CLs group, and more strong fluorescence was observed in cells treated with PFUS of 10% duty cycles. However, almost no fluorescence was detected in images of the P-CLs group despite of different duty cycles. The results indicated that PC-CLs had good ability to generate ROS under PFUS with appropriate duty cycle, and Ce6 maybe the key to generate ROS. For the consistency of experimental condition, we may choose a duty cycle of 10% in the subsequent study.

As shown in the CLSM images in Figure 4B, the viable and dead cells were displayed green fluorescence and red fluorescence respectively. No or negligible red fluorescence were seen in various groups in the absence of PFUS, while a number of red fluorescence was clearly detected in groups with PFUS. Among these groups, most dead cells were found in the PC-CLs treated group after PFUS as indicated by the massive red fluorescence. Similarly, the CLSM result was consistent with cells viability rates determined by counting (Figure 4C). From the above results, it can be concluded that no detectable cell cytotoxicity of Ce6 in this study, good biocompatibility of PC-CLs and highly efficient SDT in the presence of PC-CLs with PFUS.

Synergistic effect of PC-CLs with PFUS

After PFUS, the grayscale of target region of each group changed to different degrees in US images, and the one of PC-CLs group was more obvious than that of PBS group and B. *bifidum* group (Figure 5A). The necrotic morphology of liver tissue was elliptical in shape with different degrees of chylous inside (Figure 5C).

The grayscale value change and necrotic volume were analyzed furtherly. It could be seen from Figures 5B,D that the changes of grayscale value and necrotic volume for the PC-CLs group were both significantly greater than that of the PBS and B. *bifidum* group, indicating that PC-CLs could enhance PFUS ablation remarkably.

Targeted detection of bio-targeted ROS producing synergists

The number of colonies determined the distribution of B. *bifidum* in the tissue after gram staining. As shown in Figure 6A, no blue-stained B. *bifidum* was detected in various tissue of control group. After injection of B. *bifidum*, the B. *bifidum* steadily colonized

over time at tumor sites while gradually decreasing in other organs, indicating that B. *bifidum* first distributed throughout the body and finally targeted tumor and continuously proliferated itself. It suggested that B. *bifidum* can be used as a tumor-targeting carrier.

PC-CLs were labeled with red fluorescence to confirm the tumor-targeting of the bio-targeted ROS producing synergist (Figure 6B). Compared to non-targeted group without B. *bifidum*, there were a number of PC-CLs in the tumor of target region at 12 h after injection, suggesting that the B. *bifidum* facilitate the homing and retain of PC-CLs in tumor, and construct the bio-targeted ROS producing synergist and achieve tumor targeting *in vivo*.

Synergistic therapy of B. *bifidum*@PC-CLs with PFUS

PFUS sonication time was chosen at 12 h after PC-CLs injection for the maximum concentration of NPs observed in the tumor.

The grayscale changes (Figures 7A,B) and the necrosis volume (Figures 7C,D) of B. *bifidum* group and PC-CLs group were higher than those of the PBS groups, indicating that both B. *bifidum* and PC-CLs could enhance PFUS ablation. The higher the ablation efficiency, the smaller the value of EEF. Figure 7E showed that the B. *bifidum*, PC-CLs and the B. *bifidum*@PC-CLs group had significantly lower EEF than the PBS group, the one of B. *bifidum*@PC-CLs was the most obvious. The results of *in vivo* tumor ablation experiments all proved that B. *bifidum*@PC-CLs could be used as a bio-targeted synergist in PFUS treatment.

Antitumor effect of B. *bifidum*@PC-CLs with PFUS

Figure 8 depicts the antitumor effect *in vivo* after synergistic therapy subsequently. The changes in RTV were continuously recorded. The growth trend of tumor in the group of B. *bifidum*@PC-CLs was the slowest and decreased at last, indicating an outstanding tumor inhibition effect (Figure 8B). The tumors after peeling were measured and analyzed on day 17, B. *bifidum*@PC-CLs group had the smallest tumor volume and the most apparent tumor inhibition achievement, which confirmed the obvious antitumor capability of B. *bifidum*@PC-CLs with PFUS (Figures 8A, C).

As shown in Figure 8D, HE staining images also revealed the similar results, compared to PBS group, other groups showed different nuclear pyroptosis, fragmentation and nucleolysis, and among which, group B. *bifidum*@PC-CLs was the most obvious. In Ki67 staining, tumor proliferating cell's nucleus appear brown. Apoptotic cells are labeled red by TUNEL fluorescence staining. The scope of proliferative cells in each group ranged from high to low (PBS group, B. *bifidum* group, PC-CLs group, B. bifidum@PC-CLs group). On the contrary, the scope of apoptotic cells in each group ranged from low to high according to above groups. No matter whether Ki67 or TUNEL results, bio-targeted ROS producing synergist group showed an excellent antitumor effect.

Biosafety assessment

As shown in Figure 9A, only minor hemolysis rates (less than 5%) were observed when the PC-CLs concentration was within the experimental range, providing safe confidence for testing *in vivo*. The blood indexes after B. *bifidum*@PC-CLs injection were similar to control group finally, indicating well biosafety to mice in this study (Figure 9B). Moreover, no obvious structural damage was observed in major organs of the mice in the B. *bifidum*@PC-CLs group compared to the untreated mice (Figure 9C).

Discussion

Multifunctional synergist with advanced multimodal-imaging, drug delivery, and monitoring of therapeutic is currently a hot topic in tumor diagnosis and treatment, NPs delivery system with good tumor-targeting is the core to achieve the above effects (Wang et al., 2023; Gao et al., 2024; Liu et al., 2024). Numerous studies have confirmed that B. *bifidum* could continuously attract NPs through different manners to the targeted tumor tissue for enhancing tumor therapy effect (Chen et al., 2020; Jiang et al., 2022; Li et al., 2022a). At first, the hypoxic environment inside the tumor promotes the growth of anaerobic B. *bifidum*, it proliferate the tumor target area, which can be employed as a target. Moreover, the abnormal high pressure in tumor prevents immune components from entering into the tumor, which provides a protection for B. *bifidum* (Theys et al., 2003). Because PC-CLs contains DC-CHOL, so the surface potential was positive (Wang et al., 2020a), which is opposite to the B. *bifidum*, so it can be connected by electrostatic adsorption. B. *bifidum* successfully coupled with PC-CLs by capturing PC-CLs, thereby constructed a novel bio-targeted synergist.

By virtue of the cavitation effect and thermal effect as generated by PFUS, PFH was induced to liquid-gas phase transition, generating a large number of microbubbles, which not only achieved the contrast-enhanced US imaging (Wang et al., 2024; Namen et al., 2021), but also enhance PFUS treatment as the cavitation nuclei in the targeted tissues. The introduction of Ce6 endowed the bio-targeted ROS producing NPs with excellent PA and FL imaging capabilities. With the addition of two imaging modes, the original US imaging can be enriched, the structures and functions of tissue can be visualized (Xu et al., 2023), while the drug delivery is more sensitive and accurate (Zeng et al., 2021). The PFUS was performed under multi-mode imaging, the most effective therapy result can be achieved because of the chosen treatment time.

PFUS-SDT combined enhanced treatment and antitumor effect significantly. As a type of ultrasound, PFUS can accurately excite Ce6 to release ROS for its good penetration ability. ROS can activate autophagy and apoptosis through various specific mechanisms, which ultimately result in DNA damage and cell death in target area (Afifi et al., 2023). PFUS with different duty cycles will allow drug of different amount to be delivered (Yang et al., 2023; Pan et al., 2005; Svenja et al., 2023). Experiment results in the study revealed that PFUS with a duty cycle of 10% can stimulate PC-CLs to produce a large amount of ROS and promote 4T1 tumor cell death, which provided an optimized therapy parameter for subsequent PFUS-SDT tumor treatment *in vivo*.

Group B. *bifidum*@PC-CLs achieved excellent therapy effect, which may be related to the following reasons. PFH could cause cavitation effect and mechanical effect in PFUS treatment to destroy tumor tissue because of its phase transition characteristics (Rajabi et al., 2023; Tang et al., 2021). B. *bifidum*, as a biological targeting carrier to tumors, not only could change the acoustic environment at the targeted tumor, but also greatly improve the concentration of NPs. That was the reason that the treatment efficacy of group B. *bifidum* or group PC-CLs was higher than that of group PBS. Therefore, the combination of the effects above realized the biological targeting synergism. Compared with PBS group, the B. *bifidum* group also inhibited tumor growth. It was reported that Bifidobacterium, even its products, could play beneficial pleiotropic effects on the immune system, including the activating of tumor-specific IL-12, IFN-γ and $CD8^+$ cytolytic responses that inhibit tumor growth (Cao et al., 2024; Wang et al., 2025), however, the benefit was limited. Although ROS released at tumor area in group PC-CLs, the SDT effect was still inferior to that in group B. *bifidum*@PC-CLs. Because the bio-targeted ROS producing synergist could not only realize inhibit-tumor effect during biological tumor targeting, but also increase the ROS at tumor area, improved SDT effect, and achieved PFUS-SDT combined therapy with high efficiency.

Conclusion

Such a bio-targeted ROS producing synergist with the combination of real-time multimodal imaging and SDT would be of great value to address the drawbacks of current therapies, showing great potential as a unique nanoparticle platform to guide PFUS for efficient and safety tumor treatment.

Data availability statement

The original contributions presented in the study are included in the article/supplementary material, further inquiries can be directed to the corresponding authors.

Ethics statement

The animal study was approved by the Animal Care Institution of Chongqing Medical University. The study was conducted in accordance with the local legislation and institutional requirements.

Author contributions

XO: Data curation, Methodology, Writing – original draft, Supervision, Writing – review and editing. YT: Project administration, Validation, Writing – original draft. HY: Funding acquisition, Software, Writing – review and editing. YD: Formal Analysis, Investigation, Writing – original draft. ZZ: Software, Validation, Writing – original draft. LL: Conceptualization, Validation, Writing – original draft. QW: Data curation, Methodology, Writing – original draft. JZ: Project administration, Resources, Supervision, Writing – review and editing.

Funding

The author(s) declare that financial support was received for the research and/or publication of this article. Chongqing Postdoctoral Research Project (2023CQBSHTB1005).

Conflict of interest

The authors declare that the research was conducted in the absence of any commercial or financial relationships that could be construed as a potential conflict of interest.

The reviewer DW declared a shared parent affiliation with the authors to the handling editor at the time of review.

Generative AI statement

The author(s) declare that no Generative AI was used in the creation of this manuscript.

Publisher's note

All claims expressed in this article are solely those of the authors and do not necessarily represent those of their affiliated organizations, or those of the publisher, the editors and the reviewers. Any product that may be evaluated in this article, or claim that may be made by its manufacturer, is not guaranteed or endorsed by the publisher.

References

Afifi, M. M., El-Gebaly, R. H., Abdelrahman, I. Y., and Rageh, M. M. (2023). Efficacy of iron-silver bimetallic nanoparticles to enhance radiotherapy. *N-S Arch. Pharmacol.* 396 (12), 3647–3657. doi:10.1007/s00210-023-02556-9

Benito, I., Encío, I. J., Milagro, F. I., Alfaro, M., Martínez-Peñuela, A., Barajas, M., et al. (2021). Microencapsulated bifidobacterium bifidum and lactobacillus gasseri in combination with quercetin inhibit colorectal cancer development in ApcMin/+ mice. *Int. J. Mol. Sci.* 22 (9), 4906. doi:10.3390/ijms22094906

Cao, L., Wang, X., Ma, X., Xu, M., and Li, J. (2024). Potential of natural products and gut microbiome in tumor immunotherapy. *Chin. Med.* 19 (1), 161. doi:10.1186/s13020-024-01032-7

Chen, C., Wang, Y., Tang, Y., Wang, L., Jiang, F., Luo, Y., et al. (2020). Bifidobacterium-mediated high-intensity focused ultrasound for solid tumor therapy: comparison of two nanoparticle delivery methods. *Int. J. Hyperther* 37 (1), 870–878. doi:10.1080/02656736.2020.1791365

Cheng, C., Jiang, W., Luo, Y., Wan, L., Guo, X., Xie, Z., et al. (2023). Nir activated multimodal therapeutics based on metal-phenolic networks-functionalized nanoplatform for combating against multidrug resistance and metastasis. *Small* 19 (14), e2206174. doi:10.1002/smll.202206174

Dong, H., Li, Q., Zhang, Y., Ding, M., Teng, Z., and Mou, Y. (2023). Biomaterials facilitating dendritic cell-mediated cancer immunotherapy. *Adv. Sci. (Weinh)* 10 (18), e2301339. doi:10.1002/advs.202301339

Fukiya, S., Hirayama, Y., Sakanaka, M., Kano, Y., and Yokota, A. (2012). Technological advances in bifidobacterial molecular genetics: application to functional genomics and medical treatments. *Biosci. Microbiota Food Health* 31 (2), 15–25. doi:10.12938/bmfh.31.15

Gao, Y., Luo, Y., Chen, W., Xue, X., Xiao, C., and Wei, K. (2024). Theranostic nanoplatform based on polydopamine-coated magnetic mesoporous silicon for precise cancer triplex nanotherapy and multimodal imaging. *Anal. Chem.* 96 (33), 13557–13565. doi:10.1021/acs.analchem.4c02244

He, Z., Tian, S., Gao, Y., Meng, F., and Luo, L. (2021). Luminescent AIE dots for anticancer photodynamic therapy. *Front. Chem.* 9, 672917. doi:10.3389/fchem.2021.672917

Huang, Y., Ouyang, W., Lai, Z., Qiu, G., Bu, Z., Zhu, X., et al. (2024). Nanotechnology-enabled sonodynamic therapy against malignant tumors. *Nanoscale Adv.* 6 (8), 1974–1991. doi:10.1039/d3na00738c

Ippolito, L., Morandi, A., Giannoni, E., and Chiarugi, P. (2019). Lactate: a metabolic driver in the tumour landscape. *Trends Biochem. Sci.* 44 (2), 153–166. doi:10.1016/j.tibs.2018.10.011

Jian, J., Liu, C., Gong, Y., Su, L., Zhang, B., Wang, Z., et al. (2014). India ink incorporated multifunctional phase-transition nanodroplets for photoacoustic/ultrasound dual-modality imaging and photoacoustic effect based tumor therapy. *Theranostics* 4 (10), 1026–1038. doi:10.7150/thno.9754

Jiang, F., Wang, L., Tang, Y., Wang, Y., Li, N., Wang, D., et al. (2022). US/MR bimodal imaging-guided bio-targeting synergistic agent for tumor therapy. *Int. J. Nanomedicine* 17, 2943–2960. doi:10.2147/IJN.S363645

Khella, K. F., Abd El Maksoud, A. I., Hassan, A., Abdel-Ghany, S. E., Elsanhoty, R. M., Aladhadh, M. A., et al. (2022). Carnosic acid encapsulated in albumin nanoparticles induces apoptosis in breast and colorectal cancer cells. *Molecules* 27 (13), 4102. doi:10.3390/molecules27134102

Kikuchi, T., Shimizu, H., Akiyama, Y., and Taniguchi, S. (2017). *In situ* delivery and production system of trastuzumab scFv with Bifidobacterium. *Biochem. Bioph Res. Co.* 493 (1), 306–312. doi:10.1016/j.bbrc.2017.09.026

Kim, H., Chae, S., Lee, M., Yang, S., Ban, O., Jung, Y., et al. (2021). Genomic and toxicity studies on Bifidobacterium bifidum IDCC 4201 and Bifidobacterium longum IDCC 4101 isolated from feces of breast-fed infants. *Food Suppl. Biomater. Health* 1 (4). doi:10.52361/fsbh.2021.1.e37

Kim, S., Lee, H. H., Choi, W., Kang, C. H., Kim, G. H., and Cho, H. (2022). Anti-tumor effect of heat-killed Bifidobacterium bifidum on human gastric cancer through Akt-p53-dependent mitochondrial apoptosis in xenograft models. *Int. J. Mol. Sci.* 23 (17), 9788. doi:10.3390/ijms23179788

Li, D. S., Kripfgans, O. D., Fabiilli, M. L., Brian, F. J., and Bull, J. L. (2014). Initial nucleation site formation due to acoustic droplet vaporization. *Appl. Phys. Lett.* 104 (6), 063703. doi:10.1063/1.4864110

Li, S., Wei, Y., Zhang, B., and Li, X. (2023). Research progress and clinical evaluation of histotripsy: a narrative review. *Ann. Transl. Med.* 11 (6), 263. doi:10.21037/atm-22-2578

Li, W., Zhang, S., Xing, D., and Qin, H. (2022a). Pulsed microwave-induced thermoacoustic shockwave for precise glioblastoma therapy with the skin and skull intact. *Small* 18 (25), e2201342. doi:10.1002/smll.202201342

Li, W., Zhang, Z., Liu, J., Wang, B., Pu, G., Li, J., et al. (2022b). Nanodrug-loaded Bifidobacterium bifidum conjugated with anti-death receptor antibody for tumor-targeted photodynamic and sonodynamic synergistic therapy. *Acta Biomater.* 146, 341–356. doi:10.1016/j.actbio.2022.05.016

Liu, X., Tan, Y., Zhang, J., Huang, W., Yan, D., Wang, D., et al. (2024). Structural modulation of aggregation-induced emission luminogens for NIR-II fluorescence imaging/photoacoustic imaging of tumors. *Chem. Sci.* 15 (32), 12957–12963. doi:10.1039/d4sc01721h

Luo, Y., Xu, D., Gao, X., Xiong, J., Jiang, B., Zhang, Y., et al. (2019). Nanoparticles conjugated with bacteria targeting tumors for precision imaging and therapy. *Biochem. Biophys. Res. Co.* 514, 1147–1153. doi:10.1016/j.bbrc.2019.05.074

Luo, Y. L., Qiao, B., Yang, C., Zhang, P., Xie, Z., Cao, J., et al. (2022). Low intensity focused ultrasound ignited "Deep-penetration nanobomb" (DPNB) for tetramodal imaging guided hypoxia-tolerant sonodynamic therapy against hypoxic tumors. *Int. J. Nanomedicine* 17, 4547–4565. doi:10.2147/IJN.S361648

Mai, X., Chang, Y., You, Y., He, L., and Chen, T. (2021). Designing intelligent nano-bomb with on-demand site-specific drug burst release to synergize with high-intensity focused ultrasound cancer ablation. *J. Control Release* 331, 270–281. doi:10.1016/j.jconrel.2020.09.051

Martino, E., D'Onofrio, N., Anastasio, C., Abate, M., Zappavigna, S., Caraglia, M., et al. (2023). MicroRNA-nanoparticles against cancer: opportunities and challenges for personalized. *Mol. Ther. Nucleic Acids* 32, 371–384. doi:10.1016/j.omtn.2023.03.021

Mcgranahan, N., and Swanton, C. (2017). Clonal heterogeneity and tumor evolution: past, present, and the future. *Cell* 168 (4), 613–628. doi:10.1016/j.cell.2017.01.018

Namen, A. V., Jandhyala, S., Jordan, T., and Luke, G. P. (2021). Repeated acoustic vaporization of perfluorohexane nanodroplets for contrast-enhanced ultrasound imaging. *IEEE Tultrason Ferr.* 68 (12), 3497–3506. doi:10.1109/tuffc.2021.3093828

Ou, X., Zhang, Z., Lin, L., Du, Y., Tang, Y., Wang, Y., et al. (2023). Tumor-homing bacterium-adsorbed liposomes encapsulating perfluorohexane/doxorubicin enhance pulsed-focused ultrasound for tumor therapy. *RSC Adv.* 13, 19065–19078. doi:10.1039/d3ra01876h

Pan, H., Zhou, Y., Izadnegahdar, O., Cui, J., and Deng, C. X. (2005). Study of sonoporation dynamics affected by ultrasound duty cycle. *Ultrasound Med. Biol.* 31 (6), 849–856. doi:10.1016/j.ultrasmedbio.2005.03.014

Qiu, Y., Wu, Z., Chen, Y., Liao, J., Zhang, Q., Wang, Q., et al. (2023). Nano ultrasound contrast agent for synergistic chemo-photothermal therapy and enhanced immunotherapy against liver cancer and metastasis. *Adv. Sci. (Weinh)* 10 (21), e2300878. doi:10.1002/advs.202300878

Rajabi, A., Mogheiseh, A., Nazifi, S., Ahrari-Khafi, M., Dehghanian, A., Vesal, N., et al. (2023). Effect of direct therapeutic ultrasound exposure of ovaries on histopathology, inflammatory response, and oxidative stress in dogs. *BMC Vet. Res.* 19 (1), 88. doi:10.1186/s12917-023-03657-6

Ran, X., Chen, P., Liu, Y., Shi, L., Chen, X., Liu, Y., et al. (2023). Rational design of polymethine dyes with NIR-II emission and high photothermal conversion efficiency for multimodal-imaging-guided photo-immunotherapy. *Adv. Mater* 35, e2210179. doi:10.1002/adma.202210179

Ruger, L. N., Hay, A. N., Vickers, E. R., Coutermarsh-Ott, S. L., Gannon, J. M., Covell, H. S., et al. (2023). Characterizing the ablative effects of histotripsy for osteosarcoma: *in vivo* study in dogs. *Cancers (Basel)* 15 (3), 741. doi:10.3390/cancers15030741

Shan, T., Wang, W., Fan, M., Bi, J., He, T., Sun, Y., et al. (2024). Effective glioblastoma immune sonodynamic treatment mediated by macrophage cell membrane cloaked biomimetic nanomedicines. *J. Control Release* 370, 866–878. doi:10.1016/j.jconrel.2024.04.043

Shi, H., Chen, L., Liu, Y., Wen, Q., Lin, S., Wen, Q., et al. (2023). Bacteria-driven tumor microenvironment-sensitive nanoparticles targeting hypoxic regions enhances the chemotherapy outcome of lung cancer. *Int. J. Nanomedicine* 18, 1299–1315. doi:10.2147/IJN.S396863

Svenja, M., Jhansi, H. A., Samantha, M. A., Dean, M. Z., Ji, J., Wright, G., et al. (2023). Investigating the influence of ultrasound parameters on ibuprofen drug release from hydrogels. *Drug Deliv. Transl. Re* 13 (5), 1390–1404. doi:10.1007/s13346-022-01277-5

Tang, Y., Chen, L., Zhang, A., Liao, C., Gross, M. E., and Kim, E. S. (2021). *In vivo* non-thermal, selective cancer treatment with high-frequency medium-intensity focused ultrasound. *IEEE Access* 9, 122051–122066. doi:10.1109/access.2021.3108548

Theys, J., Barbé, S., Landuyt, W., Nuyts, S., Van, M. L., Wouters, B., et al. (2003). Tumor-specific gene delivery using genetically engineered bacteria. *Curr. Gene Ther.* 3 (3), 207–221. doi:10.2174/1566523034578357

Tian, S., Li, J., Wang, D., Han, Y., Dai, H., and Yan, L. (2024). Sonodynamic-chemotherapy synergy with chlorin e6-based carrier-free nanoparticles for non-small cell lung cancer. *J. Mater Chem. B* 12 (13), 3282–3291. doi:10.1039/d4tb00009a

Wang, H., Baba, Y., Hara, Y., Hara, Y., Kosumi, K., Harada, K., et al. (2025). The relationship between gut microbiome bifidobacterium and anti-tumor immune responses in esophageal squamous cell carcinoma. *Ann. Surg. Oncol.* 32, 3828–3838. doi:10.1245/s10434-024-16288-4

Wang, S., He, H., Mao, Y., Zhang, Y., and Gu, N. (2024). Advances in atherosclerosis theranostics harnessing iron oxide-based nanoparticles. *Adv. Sci. (Weinh)* 1 (17), e2308298. doi:10.1002/advs.202308298

Wang, Y., Chen, C., Luo, Y., Xiong, J., Tang, Y., Yang, H., et al. (2020b). Experimental study of tumor therapy mediated by multimodal imaging based on a biological targeting synergistic agent. *J. Nanobiotechnology* 15, 1871–1888. doi:10.2147/IJN.S238398

Wang, Y., Wang, Q., Luo, Y., Jiang, L., Zeng, Z., Gan, L., et al. (2020a). Comparative study of pulsed versus continuous high-intensity focused ultrasound ablation using *in vitro* and *in vivo* models. *J. Ultras Med.* 39 (2), 259–271. doi:10.1002/jum.15098

Wang, Y., Zhang, Z., Ren, L., Luo, Y., Wang, Q., and Zou, J. (2023). Dual mode imaging guided multi-functional bio-targeted oxygen production probes for tumor therapy. *J. Nanobiotechnology* 21 (1), 142–161. doi:10.1186/s12951-023-01901-7

Xu, N., Wu, D., Gao, J., Jiang, H., Li, Q., Bao, S., et al. (2023). The effect of tumor vascular remodeling and immune microenvironment activation induced by radiotherapy: quantitative evaluation with magnetic resonance/photoacoustic dual-modality imaging. *Quant. Imag. Med. Surg.* 13 (10), 6555–6570. doi:10.21037/qims-23-229

Yang, W., Veroniaina, H., Qi, X., Chen, P., Li, F., and Ke, P. C. (2020). Soft and condensed nanoparticles and nanoformulations for cancer drug delivery and repurpose. *Adv. Ther. (Weinh).* 3 (1), 1900102. doi:10.1002/adtp.201900102

Yang, Y., Huang, J., Liu, M., Qiu, Y., Chen, Q., Zhao, T., et al. (2023). Emerging sonodynamic therapy-based nanomedicines for cancer immunotherapy. *Adv. Sci. (Weinh)* 10 (2), e2204365. doi:10.1002/advs.202204365

Zeng, W., Yu, Q., Wang, D., Liu, J., Yang, Q., Zhou, Z., et al. (2021). Mitochondria-targeting graphene oxide nanocomposites for fluorescence imaging-guided synergistic phototherapy of drug-resistant osteosarcoma. *J. Nanobiotechnology* 9 (1), 79. doi:10.1186/s12951-021-00831-6

Zeng, Z., Liu, J. B., and Peng, C. Z. (2022). Phase-changeable nanoparticle-mediated energy conversion promotes highly efficient high-intensity focused ultrasound ablation. *Curr. Med. Chem.* 29 (8), 1369–1378. doi:10.2174/0929867328666210708085110

Zhang, D., Liu, S., Guan, J., and Mou, F. (2022). Motile-targeting drug delivery platforms based on micro/nanorobots for tumor therapy. *Front. Bioeng. Biotechnol.* 10, 1002171. doi:10.3389/fbioe.2022.1002171

Zhao, P., Tian, Y., Lu, Y., Zhang, J., Tao, A., Xiang, G., et al. (2022). Biomimetic calcium carbonate nanoparticles delivered IL-12 mRNA for targeted glioblastoma sono-immunotherapy by ultrasound-induced necroptosis. *J. Nanobiotechnology* 20 (1), 525. doi:10.1186/s12951-022-01731-z